Non-Double-Couple Moment Tensors of Earthquakes Calculated Using Empirical Green's Functions

Václav Vavryčuk*[1] and Petra Adamová[1]

Abstract

We present a joint inversion for empirical Green's functions (EGFs) and high-resolution non-double-couple (non-DC) moment tensors. First, the EGFs are constructed using known moment tensors of earthquakes occurring in a small focal zone. Second, the estimated EGFs are applied to refine the original moment tensors used for constructing the EGFs. Because the EGFs describe the velocity model better than the standard GFs, the refined moment tensors are more accurate. The method is applied to real observations of earthquakes of the 2008 swarm in West Bohemia, Czech Republic, where tiny details in fracturing in the focal zone are revealed. Refined moment tensors indicate fault closing caused by compaction of fault gouge during fracturing process related to fault weakening by fluids in the focal zone. The application of the proposed inversion can improve moment tensors reported in existing local, regional, or global catalogs for areas with a concentrated seismicity.

Cite this article as Vavryčuk, V., and P. Adamová (2019). Non-Double-Couple Moment Tensors of Earthquakes Calculated Using Empirical Green's Functions, *Seismol. Res. Lett.* **91**, 390–398, doi: 10.1785/0220190154.

Introduction

Determination of reliable moment tensors is difficult, because it requires observations from many stations, good station coverage of the focal zone, accurate locations, and a detailed velocity model needed for calculating Green's functions (Vavryčuk, 2007; Šílený, 2009; Ford *et al.*, 2010; Stierle, Bohnhoff, and Vavryčuk, 2014; Stierle, Vavryčuk, *et al.*, 2014). If details of the model are unknown, the inversion must be confined to low frequencies (Dziewonski *et al.*, 1981, 2001; Minson and Dreger, 2008; Sokos and Zahradník, 2008) that are insensitive to small-scale heterogeneities, and the moment tensors are estimated only roughly. A way to manage the problem with a complex structure characterized by unknown 3D heterogeneities, attenuation, or anisotropy (Šílený and Vavryčuk, 2002), is to construct the so-called empirical Green's functions (EGFs), see Hartzell (1978), Kanamori (1979), and Irikura (1983). In this approach, weak earthquakes occurring along a fault are assumed to provide complete transfer properties from the focal zone to a given station. Assuming some rupture history of large earthquakes along a fault, their wavefields can be computed by summing contributions from individual EGFs. Alternatively, the rupture history can be calculated from the EGFs and from observations of a large earthquake. The method is, however, approximate, because all earthquakes, weak or large, must have the same focal mechanisms. Because faults display irregularities and may consist of many differently oriented fault segments, this assumption is, however, often violated.

A significant improvement of the EGF method was proposed by Plicka and Zahradník (1998) who developed a method for calculating the so-called empirical Green's tensor spatial derivatives with no *a priori* assumption about the similarity of focal mechanisms of weak earthquakes. Instead, selected well-recorded weak earthquakes are first inverted for moment tensors in a standard way, and secondly, the EGFs (or more accurately the empirical Green's tensor spatial derivatives) are inverted from observed waveforms of the weak earthquakes and from their moment tensors. The computed EGFs can serve for calculating moment tensors and source time functions of other weak or large earthquakes occurring in the same focal zone. Since Plicka and Zahradník (1998) computed the EGFs from earthquakes described by shear focal mechanisms, they could invert records of the other earthquakes for shear focal mechanisms only. This approach found applications in earthquake studies in various seismically active regions (Plicka and Zahradník, 2002; Ide *et al.*, 2007; Liao and Huang, 2008; Suzuki and Iwata, 2009; Ohori and Hisada, 2011).

In this article, we modify the approach of Plicka and Zahradník (1998) and introduce two extensions of their method. First, we construct the EGFs using events described by complete moment tensors but not just by their double-couple (DC) parts. Second, we show that the found EGFs

1. Institute of Geophysics, Czech Academy of Sciences, Prague, Czech Republic
*Corresponding author: vv@ig.cas.cz

© Seismological Society of America

Downloaded from https://pubs.geoscienceworld.org/ssa/srl/article-pdf/91/1/390/4910569/srl-2019154.1.pdf
by Geofyzikalni Ustav Av Cr user

can be applied even to refining the original moment tensors used for constructing the EGFs. The efficiency of the method is demonstrated on synthetic data as well as on real observations of shallow weak earthquakes that occurred during the 2008 earthquake swarm in West Bohemia, Czech Republic.

Method

The moment tensor inversion for one individual event is based on the following equation (Aki and Richards, 2002):

$$u_k = M_{lm} G_{kl,m}, \tag{1}$$

in which u_k is the displacement amplitude or the full displacement waveform observed at the kth one-component sensor, M_{lm} are the components of the moment tensor, and $G_{kl,m}$ is the spatial derivative along the m-axis of the Green's function for the kth sensor produced by the force along the l-axis. Equation (1) can be rewritten in the matrix form as

$$\mathbf{u} = \mathbf{G}\mathbf{m}, \tag{2}$$

in which $\mathbf{m}$ is the vector composed of six components of moment tensor $\mathbf{M}$,

$$\mathbf{m} = [\,M_{11} \quad M_{22} \quad M_{33} \quad M_{23} \quad M_{13} \quad M_{12}\,]^T, \tag{3}$$

and $\mathbf{G}$ is the $K \times 6$ matrix of the spatial derivatives of the Green's function for the kth sensor:

$$G_{k1} = G_{k1,1}, G_{k2} = G_{k2,2}, G_{k3} = G_{k3,3}, G_{k4} = G_{k2,3} + G_{k3,2},$$
$$G_{k5} = G_{k1,3} + G_{k3,1}, G_{k6} = G_{k1,2} + G_{k2,1}. \tag{4}$$

If we invert amplitudes of the P and/or S direct waves, the components of $\mathbf{G}$ are the scalar quantities. If we invert the full waveforms, the components of $\mathbf{G}$ are the vectors of amplitudes dependent on time.

For N events at the same focal zone but with various moment tensors, equation (1) can be expressed as follows:

$$\begin{bmatrix} u_k^{(1)} \\ u_k^{(2)} \\ \vdots \\ u_k^{(N)} \end{bmatrix} = \begin{bmatrix} m_1^{(1)} & m_2^{(1)} & m_3^{(1)} & m_4^{(1)} & m_5^{(1)} & m_6^{(1)} \\ m_1^{(2)} & m_2^{(2)} & m_3^{(2)} & m_4^{(2)} & m_5^{(2)} & m_6^{(2)} \\ \vdots & \vdots & \vdots & \vdots & \vdots & \vdots \\ m_1^{(N)} & m_2^{(N)} & m_3^{(N)} & m_4^{(N)} & m_5^{(N)} & m_6^{(N)} \end{bmatrix} \begin{bmatrix} G_{k1} \\ G_{k2} \\ G_{k3} \\ G_{k4} \\ G_{k5} \\ G_{k6} \end{bmatrix}, \tag{5}$$

in which k is the sequential number of a sensor, $k = 1, \ldots, K$. This equation can be used for calculating the matrix of the Green's function derivatives G_{kj}, $j = 1, \ldots, 6$, for the kth sensor from known moment tensors of N events $M_{kl}^{(n)}$ and from observed displacements $u_k^{(n)}$, $n = 1, \ldots, N$, produced by these events.

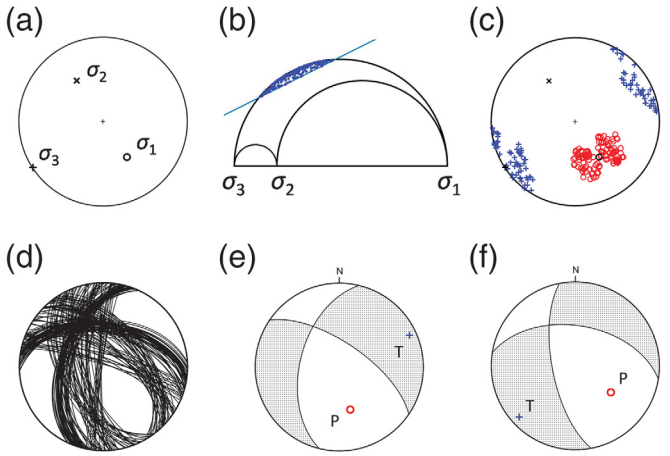

Figure 1. Noise-free focal mechanisms of 100 shear events, which satisfy the Coulomb failure criterion for given stress. (a) Directions of the principal stress axes; (b) Mohr's circle diagram; (c) distribution of the P/T axes over the focal sphere; (d) nodal lines of the noise-free focal mechanisms; and (e,f) principal focal mechanisms defined as the focal mechanisms optimally oriented for shearing under the given stress. The stress ratio is 0.8 in panel (b). The P/T axes in (c), (e), and (f) are marked by the red circles and blue plus signs, respectively.

Numerical Test

We perform synthetic tests illustrating the robustness of the proposed inversion scheme. We consider event locations, focal mechanisms, and the station configuration similar to those in the West Bohemia swarm region to mimic observations studied in the next section. In order to generate realistic focal mechanisms, we need knowledge about tectonic stress in the focal area. According to Vavryčuk (2011a, his fig. 7), the directions (azimuth/plunge) of the principal stress axes σ_1, σ_2, and σ_3 are assumed as: 146°/48°, 327°/42°, and 237°/1°, respectively (Fig. 1a). The shape ratio $R = (\sigma_1 - \sigma_2)/(\sigma_1 - \sigma_3)$ is 0.8. We calculated synthetic focal mechanisms of 100 shear earthquakes, which satisfied the Coulomb failure criterion (Fig. 1b). The P/T axes of the focal mechanisms form the so-called butterfly wings (Fig. 1c), which are observed also in real data (Vavryčuk, 2011a, his fig. 9). The butterfly wings are symmetric with respect to the stress axes, and their shape depends on fault friction and cohesion (Vavryčuk, 2011a). The nodal lines (Fig. 1d) are clustered around two principal focal mechanisms with the strike, dip, and rake angles: 304.2°, 66.4°, and −136.9° (Fig. 1e) and 169.1°, 67.6°, and −43.7° (Fig. 1f). The principal focal mechanisms are optimally oriented for shearing with respect to the tectonic stress.

The network consists of 22 stations, which surround the focal zone with foci at a depth of 8.85 km (Fig. 2a). The Green's function derivatives (Fig. 2c, black lines) needed for calculating synthetic waveforms were obtained for a layered isotropic velocity model using the discrete wavenumber method (Coutant, 1989;

Downloaded from https://pubs.geoscienceworld.org/ssa/srl/article-pdf/91/1/390/4910569/srl-2019154.1.pdf
by Geofyzikalni Ustav Av Cr user

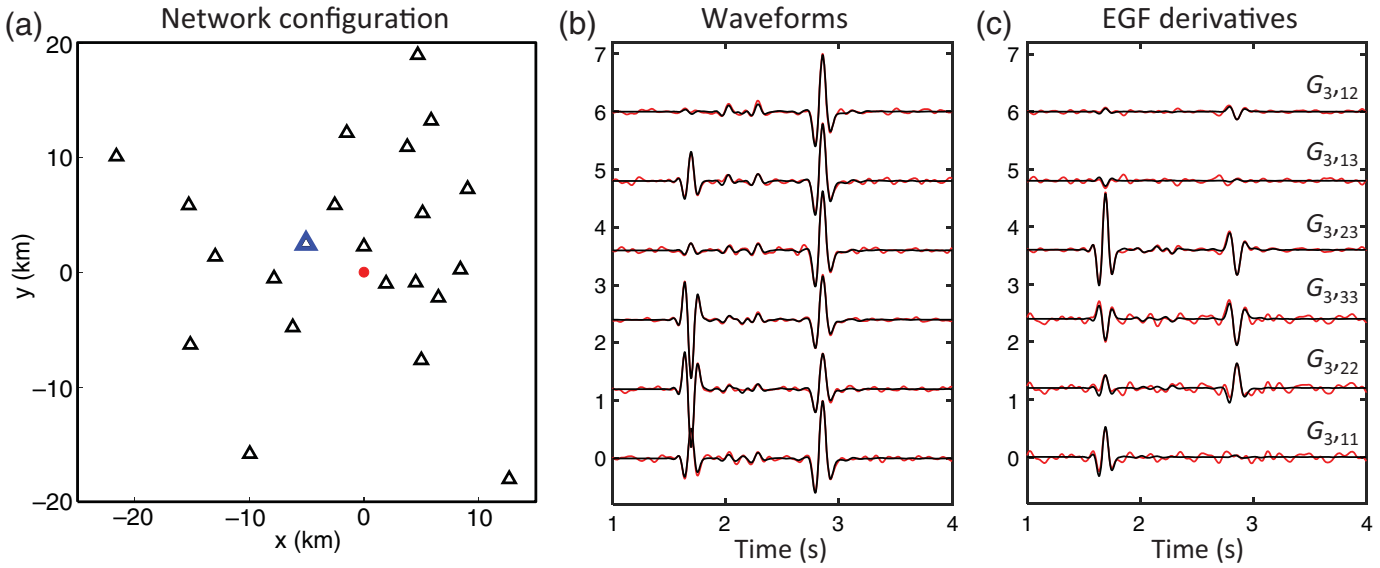

Figure 2. (a) The network configuration (black triangles); (b) vertical components of synthetic velocity records for six selected events at station marked by the blue triangle in panel (a), and (c) the empirical Green's function (EGF) derivatives at a station marked by the blue triangle in panel (a). The red dot in (a) marks the epicenter of the events. The black and red lines in (b) and (c) denote the noise-free and noisy traces, respectively.

Bouchon, 2003). Considering moment tensors of 100 shear earthquakes (Fig. 1), we computed their waveforms at all stations (Fig. 2b, black lines).

The key step is to use the synthetic waveforms contaminated by noise to simulate real observations (Fig. 2b, red lines) and moment tensors also contaminated by noise for inverting the EGF derivatives (Fig. 2c, red lines) using equation (5). The random noise in waveforms and moment tensors has a flat distribution. The maximum level of noise in waveforms is 15% of the maximum amplitude over all noise-free traces of a given event. The maximum level of noise in moment tensors is 5% of the maximum component of the noise-free moment tensor of a given event. Because of noise, the noisy moment tensors contain non-DC components: the compensated linear vector dipole (CLVD) and the isotropic component (ISO). Figure 2c shows that the true noise-free EGF derivatives (black lines) and those calculated by equation (5) (red lines) coincide well, except for noise produced by inverting noisy waveforms. Comparing Figure 2b and 2c, we see that the noise level is slightly higher in the EGF derivatives than in the original noisy waveforms.

In the next step, the calculated EGFs were applied in the moment tensor inversion of the noisy waveforms. Because the initial moment tensors used for the inversion of the EGFs were noisy, they were characterized by slightly inclined P/T axes and they contained false non-DC components (Fig. 3a,c,e). We inverted the same noisy waveforms which were used in the EGFs inversion, but we also inverted waveforms contaminated by another noise realization. In both cases, the final moment tensors obtained by the inversion using the EGFs (Fig. 3b,d,f) are less noisy and visibly closer to the true noise-free moment tensors than the initial moment tensors. This evidences that the moment tensor inversion using the EGFs is robust and not very sensitive to noise in the input data.

To simulate even a more realistic case, we varied locations of events. In contrast to Figure 2a where all events have one

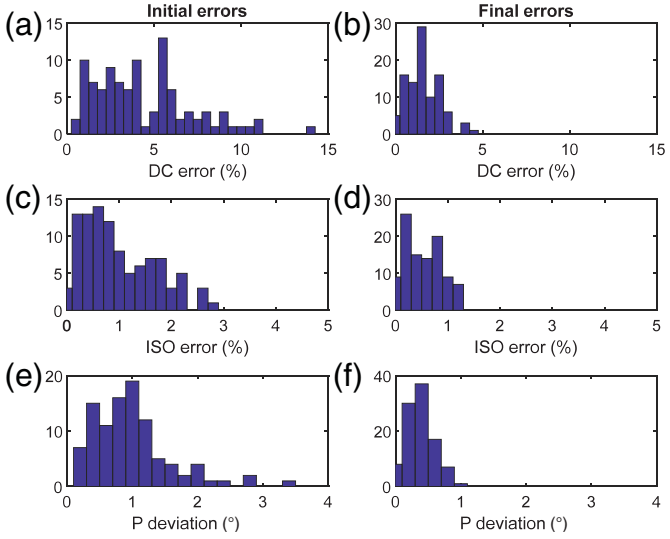

Figure 3. A comparison of (a,c,e) the initial noisy moment tensors used for constructing the EGFs and (b,d,f) the refined moment tensors calculated using the EGFs. (a,b) The errors in the double-couple (DC) percentage, (c,d) the errors in the ISO percentage, and (e,f) the errors in the deviation of the P axes. The errors are defined as the differences between the initial or final moment tensors and the true noise-free moment tensors. The DC and ISO percentages were calculated using equations (15) and (16) of Vavryčuk (2015).

Downloaded from https://pubs.geoscienceworld.org/ssa/srl/article-pdf/91/1/390/4910569/srl-2019154.1.pdf
by Geofyzikalni Ustav Av Cr user

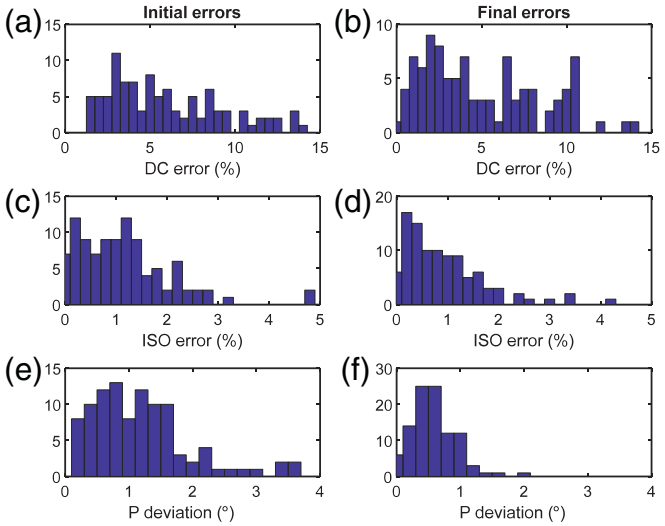

Figure 4. A comparison of (a,c,e) the initial noisy moment tensors used for constructing the EGFs and (b,d,f) the refined moment tensors calculated using the EGFs for events with varying locations. The event locations vary randomly around the originally used common focus and fill the cube with size of 200 × 200 × 200 m. For the other details, see the caption of Figure 3.

common location, we allowed the event locations to vary around the common focus by ±100 m in all three directions. The results indicate that the final moment tensors obtained using the EGFs are still less noisy than the initial moment tensors (see Fig. 4). However, comparing Figures 3 and 4 we see that the improvement is not so prominent as for the test with the common location of events. In particular, the DC errors increased if the varying locations are considered. This points to the importance of an accurate waveform alignment before the inversion and of selecting stations with distance much larger than the size of the focal zone.

The 2008 West Bohemia Swarm Earthquakes

Tectonic setting

The West Bohemia region is a geodynamically active area characterized by a frequent occurrence of earthquake swarms (Fischer *et al.*, 2014; Jakoubková *et al.*, 2018) at the same epicentral area called the Nový Kostel focal zone (Fig. 5). The seismicity occurs also in other surrounding areas, but it is weaker. Active tectonics is related to the Tertiary and Quaternary volcanism manifested by mineral springs and many degassing sites with CO_2 emanations (Kaempf *et al.*, 2013; Hrubcová *et al.*, 2017; Braeuer *et al.*, 2018). Two main fault systems, the Mariánské Lázně northwest–southeast fault and the Ore-Mountain west-southwest–east-northeast fault, characterize the tectonic structure in the area. However, the recent seismic activity is connected to the left-lateral strike-slip fault in the north–south direction, which forms the eastern boundary of the Cheb basin. Another active fault is the right-lateral strike-slip fault in the west-northwest direction. Orientations of these faults were confirmed by foci clustering and focal mechanisms (Vavryčuk *et al.*, 2013).

Seismic observations

The seismic activity is monitored by 22 local three-component seismic West Bohemia Network (WEBNET) stations (Fig. 5). The stations are distributed uniformly in the area with no significant azimuthal gaps and with epicentral distance less than 25 km (Fischer *et al.* 2010, 2014). The sampling frequency is 250 Hz, and the frequency response is flat between 1 and 60 Hz. In addition, the station with the nearest epicentral distance (station NKC) is equipped with broadband seismometer STS-2.

One of the most prominent earthquake swarms in the West Bohemia region occurred in October 2008 (Fischer *et al.*, 2010). This swarm involved about 25,000 microearthquakes of magnitudes higher than −0.5 and lasted for about four weeks. The strongest event reached a magnitude of 3.8. Accurate double-difference locations of the 2008 earthquakes reveal that geometry of the focal zone is complex (Bouchaala *et al.*, 2013; Vavryčuk *et al.*, 2013). The main active fault segment is 4 km long with a strike of N170°E. However, the main fault segment was intersected by several small differently oriented fractures. The hypocenters of 981 selected earthquakes were located at depth interval of 7.5–11 km and formed an approximately circular cloud. The density of foci along the fault is variable; the highest density is between 9.5 and 10.5 km (Fig. 6b).

Initial moment tensors

Moment tensors of the 981 located earthquakes of the 2008 swarm were calculated using the moment tensor inversion developed by Vavryčuk *et al.* (2017). The method is based on the principal component analysis (PCA) applied to the vertical components of the *P* waveforms. The PCA extracts the common wavelet, which represents the time derivative of the source time function, and the coefficients of the first principal component serve as effective amplitudes of direct *P* waves, which are inverted for the moment tensor. The method is rather insensitive to seismic noise; it is more robust than the standard amplitude inversion and applicable to large datasets.

For the purpose of this study, we selected a dense cluster of 259 foci with the size of 1 km by 1 km along the fault (Fig. 6b, red rectangle). The width of the fault is about 0.2–0.4 km. The vertical components of the *P* waves for six selected earthquakes recorded at the VAC station are shown in Figure 7a. Although the waveforms are very similar, the whole set displays a variety of focal mechanisms and indicates the presence of two wings (Fig. 8a) similar to those in the synthetic test (Fig. 1c). However, the wings are not so well separated in the real data as in the synthetic test, probably because of numerical errors in

Downloaded from https://pubs.geoscienceworld.org/ssa/srl/article-pdf/91/1/390/4910569/srl-2019154.1.pdf
by Geofyzikalni Ustav Av Cr user

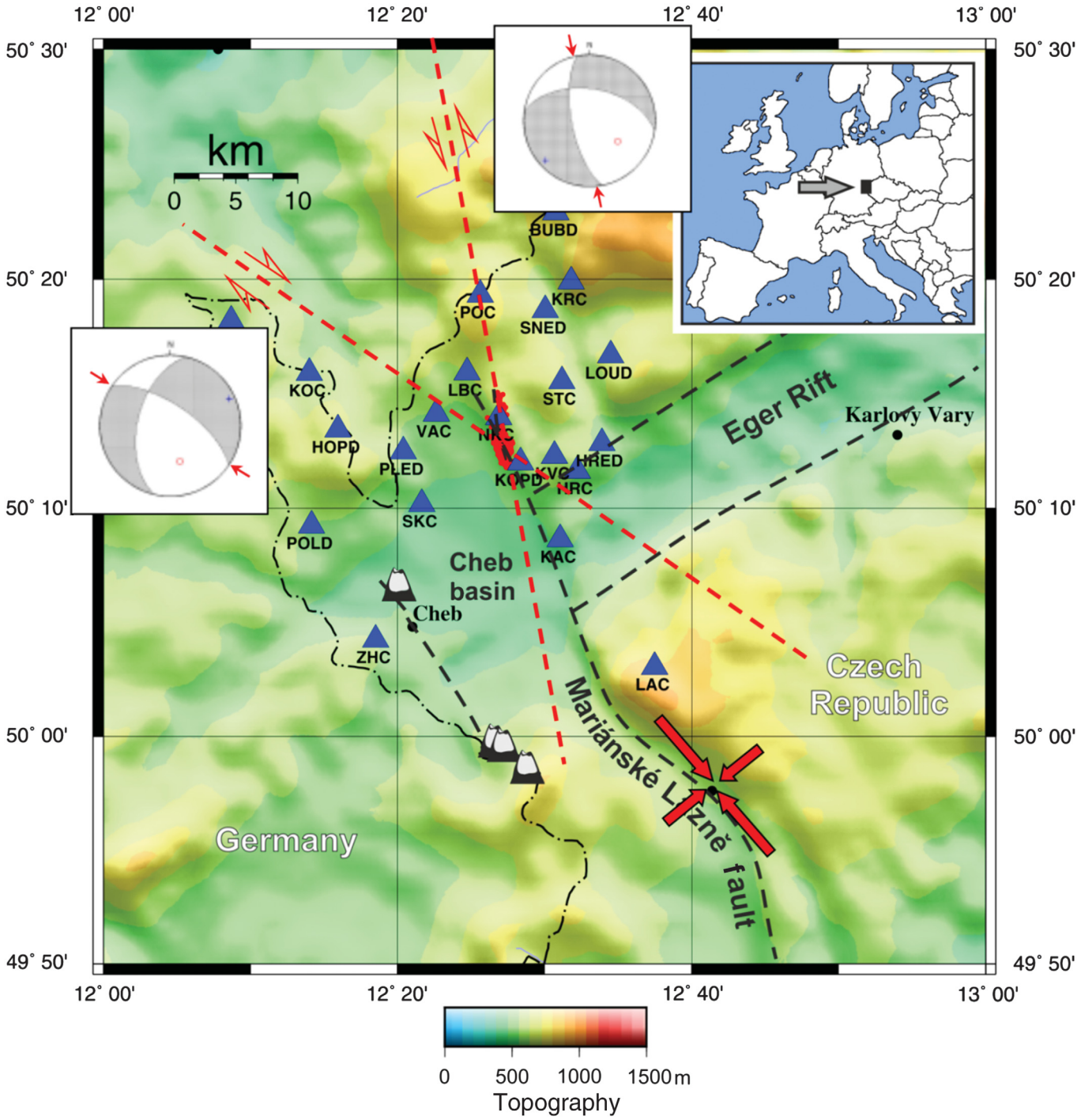

the moment tensors. Also, the non-DC components display a rather high scatter (Fig. 8c).

Moment tensors calculated using the EGFs

Even though the cluster of foci is rather small, different foci inside the cluster might produce waveforms with a variation of time delays between the *P* and *S* waves up to ~0.1 s and violate thus the assumption of identical Green's functions of the analyzed events. Therefore, we invert the *P* waveforms only, and all inverted waveforms are aligned accurately by the cross correlations (Fig. 7a). Taking into account moment tensors of

Figure 5. Topographic map of the West Bohemia region. The epicenters of the 2008 swarm earthquakes are marked by red dots. Blue triangles, the WEBNET stations; the dashed black lines, major faults; red dashed lines, calculated directions of recently active faults from focal mechanisms; full red arrows, directions of the maximum and minimum compressions; dashed–dotted line, the border between the Czech Republic and Germany. The cones show four Quaternary volcanoes in the area. The focal mechanism plots display two typical focal mechanisms observed in the region. The top right inset shows the location of the study area in Europe. After Vavryčuk and Hrubcová (2017).

Downloaded from https://pubs.geoscienceworld.org/ssa/srl/article-pdf/91/1/390/4910569/srl-2019154.1.pdf
by Geofyzikalni Ustav Av Cr user

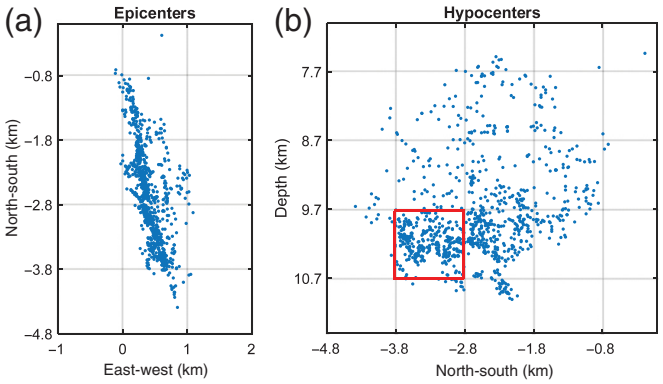

Figure 6. Foci of 981 earthquakes that occurred during 2008 earthquake swarm, calculated using the Hypo-DD method (Vavryčuk *et al.*, 2013). (a) Map view and (b) in-plane vertical section. The total of 259 earthquakes that have foci inside the red rectangle in (b) were used for calculating the EGFs.

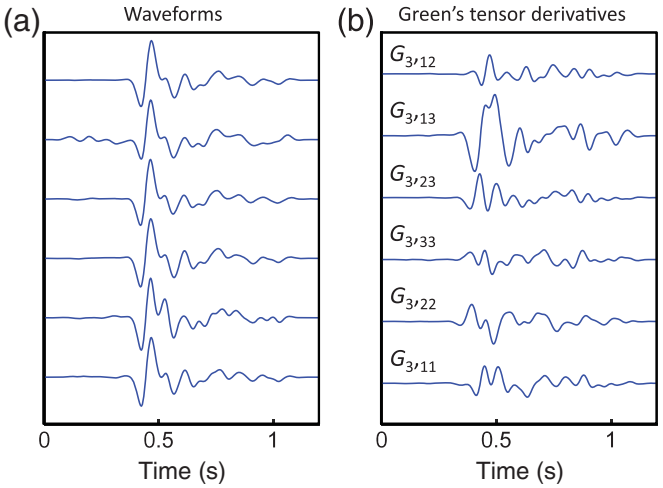

Figure 7. (a) The normalized vertical *P* waveforms recorded at the VAC station for six selected earthquakes from the total of 259 earthquakes that have foci inside the red rectangle in Figure 6b. (b) The EGF derivatives for the VAC station (for its position, see Fig. 5). The derivatives are normalized to the maximum amplitude of the strongest trace.

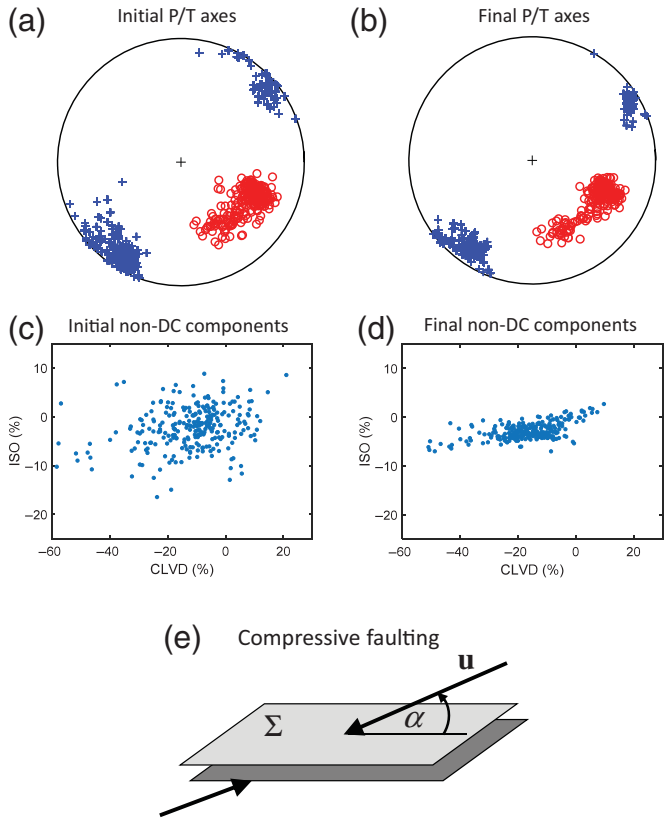

Figure 8. (a,c) Original and (b,d) refined moment tensors of the 259 earthquakes under study. (a,b) The P/T axes; (c,d) the compensated linear vector dipole-isotropic component (CLVD-ISO) plots; and (e) the scheme of compressive faulting consistent with observations of predominantly negative ISO and CLVD in panel (d). The ISO and CLVD percentages were calculated using equations (15) and (16) of Vavryčuk (2015).

the 259 analyzed earthquakes determined by the PCA-based inversion (Fig. 8a,c) and applying equation (5) to the aligned *P*-wave vertical components, we calculated the EGFs at all stations (Fig. 7b). Then we used the *P* waveforms and the EGFs (Fig. 7a,b) and refined the initial moment tensors (Fig. 8b,d). The improvement of the moment tensors calculated by the EGFs was amazing. The one elongated cluster of the original P axes divided into two subclusters corresponding to two butterfly wings. Also, the blurred and highly scattered pattern of the original non-DC components strikingly compacted almost into a line. The non-DC components of the vast majority of earthquakes are negative, indicating diminishing the volume and squeezing a material in the focal zone during the rupture process (Fig. 8e).

The robustness of the method and the stability of the refined moment tensors were further tested using differently extensive datasets for calculating the EGFs (Fig. 9). We used 104, 199, and 207 randomly selected earthquakes from the whole dataset of 259 earthquakes under study. Hence, the subsets were formed by 40%, 60%, and 80% of all earthquakes. Figure 9 indicates that the scatter of the P/T axes and of the non-DC components is lower in the refined moment tensors compared to the original ones. Nevertheless, it is clearly seen that the resolution of the results increases with increasing the number of earthquakes used in constructing the EGFs. The P axes form just one cluster in Figure 9a, but they start to be split into two clusters, when the EGFs are calculated with a higher number of earthquakes. Also the CLVD-ISO plots vary; the clusters change in their shape as well as in their position. However, in all cases, they are more compact than the cluster in the original CLVD-ISO plot.

Downloaded from https://pubs.geoscienceworld.org/ssa/srl/article-pdf/91/1/390/4910569/srl-2019154.1.pdf
by Geofyzikalni Ustav Av Cr user

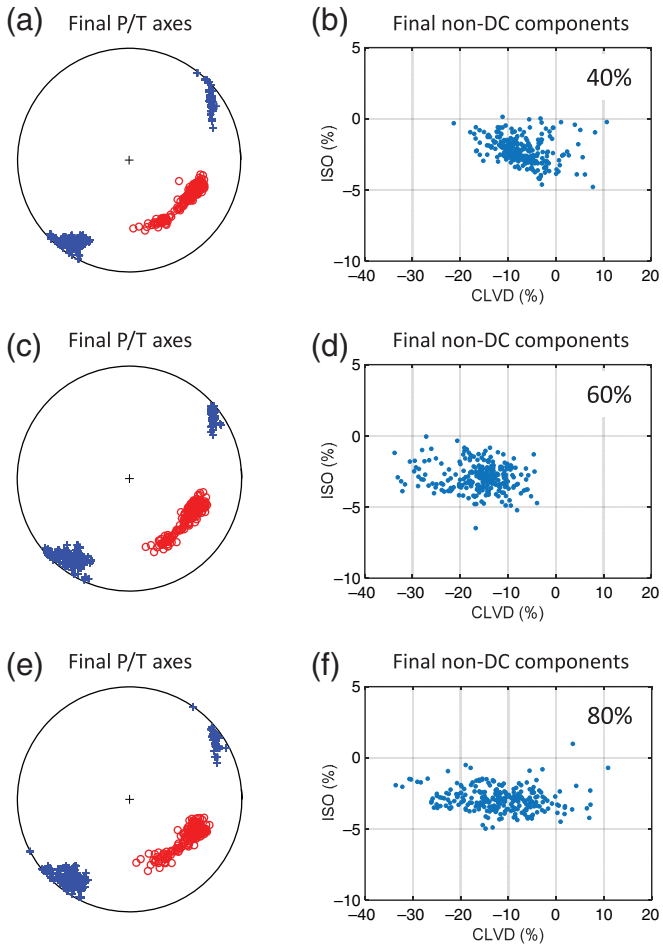

Figure 9. (a,c,e) The P/T axes and (b,d,f) the CLVD-ISO plots for the refined moment tensors of 259 earthquakes under study. The EGFs were calculated using a different number of earthquakes randomly selected from the whole dataset: (a,b) 40%, (c,d) 60%, and (e,f) 80% of 259 earthquakes under study.

Discussion and Conclusions

Originally, the EGF method was developed for studying and reconstructing wavefields of large earthquakes using waveforms of small earthquakes observed at the same focal zone and with a similar shear focal mechanism. Here we showed that the method could find other important applications. Using records of weak earthquakes and their moment tensors, we can:

- construct the EGFs for stations, which are not calibrated or which have misoriented sensors;
- determine the EGFs for stations producing complex waveforms (e.g., stations installed in sedimentary basins) affected by scattering, caustics, anisotropy, site effects, and other complexities of 3D structures;
- utilize high-frequency waveforms that contain more information than just the amplitudes of direct waves or the low-frequency waveforms used commonly in the waveform inversions; and
- invert for accurate non-DC components of moment tensors, which is extremely difficult for standard moment tensor inversions.

In this way, we can gather and utilize more information about the structure in the moment tensor inversion, and we can calculate moment tensors of much higher accuracy than when using the standard GFs. This is particularly important when retrieving the non-DC components (Julian *et al.*, 1998; Miller *et al.*, 1998), which are very sensitive to inaccurate GFs and masked frequently by numerical errors. The inversion with the EGFs is applicable not only to new earthquakes occurring in the study area but also to those used in the process of constructing the EGFs in order to refine their moment tensors.

The procedure of refining original moment tensors might look apparently impossible and physically incorrect, because the calculated EGFs should be affected by the errors of original moment tensors. However, as demonstrated on numerical tests, if a large dataset of inaccurate moment tensors is used for constructing the EGFs, random errors in the original moment tensors are suppressed, and the computed EGFs can be highly accurate. Consequently, the refined moment tensors can be more accurate than the original moment tensors. This was evidenced not only by the numerical tests but also by the analysis of real observations from West Bohemia. The analysis indicated an increase of the accuracy of the orientation of the P/T axes as well as of the amount of the non-DC components. Obviously, systematic errors in the original moment tensors cannot be eliminated by the proposed approach.

When comparing the original and refined moment tensors of the West Bohemia earthquakes, we observe that a blurred cluster of the P/T axes of the 259 original moment tensors (Fig. 8a) splits after the refinement into two subclusters (Fig. 8b), which described the so-called butterfly wings (Vavryčuk, 2011a). Also, a large ellipsoidal cluster of scattered non-DC components in the ISO-CLVD plot (Fig. 8c) compacted almost into a line (Fig. 8d). This line can straightforwardly be interpreted as a typical signature of shear-tensile faulting (Vavryčuk, 2011b). Since 95% of earthquakes have negative ISO and CLVD components, the fault gouge compacted during the rupture process and caused fault closing. Closing of the fault is probably related to fault weakening due to its erosion by fluids present in the focal zone. Faults serve as pathways for fluids, which interact with the melted rock and dissolve and alter various minerals (Heinicke *et al.*, 2009). Hence, the porosity of the fault gouge is high before the rupture process, and strength of the fault is weak. During rupturing, the fault is compacted, and its strength recovers (Vavryčuk and Hrubcová, 2017). Detecting such tiny details in rupturing is important for physical interpretations but extremely difficult to be revealed by standard moment tensor inversions.

Downloaded from https://pubs.geoscienceworld.org/ssa/srl/article-pdf/91/1/390/4910569/srl-2019154.1.pdf
by Geofyzikalni Ustav Av Cr user

The proposed generalization of the EGF method is attractive because (1) it allows the incorporation of more stations with a complicated velocity model, for which the full waveform GFs are difficult to calculate, (2) it eliminates calibration issues and misorientations of problematic sensors, and (3) it suppresses the sensitivity to unmodeled local site effects. All these attributes of the novel EGF method indicate the utility of its application in detailed studies of complex fracturing processes in active focal zones. Importantly, the method can contribute to improving moment tensors reported in existing local, regional, or global catalogs for areas with an intense and compact seismicity.

Data and Resources

The data are available at the West Bohemia Network (WEBNET) database (https://www.ig.cas.cz/en/observatories/local-seismic-network-webnet/, last accessed September 2019).

Acknowledgments

The authors thank two anonymous reviewers for their helpful comments. The study was supported by the Grant Agency of the Czech Republic, Grant Numbers 19-06422S and 17-19297S. The data are available at the West Bohemia Network (WEBNET) database or at vv@ig.cas.cz.

References

Aki, K., and P. G. Richards (2002). *Quantitative Seismology*, University Science Books, Sausalito, California.

Bouchaala, F., V. Vavryčuk, and T. Fischer (2013). Accuracy of the master-event and double-difference locations: Synthetic tests and application to seismicity in West Bohemia, Czech Republic, *J. Seismol.* **17,** no. 3, 841–859, doi: 10.1007/s10950-013-9357-4.

Bouchon, M. (2003). A review of the discrete wavenumber method, *Pure Appl. Geophys.* **160,** nos. 3/4, 445–465.

Braeuer, K., H. Kaempf, S. Niedermann, and G. Strauch (2018). Monitoring of helium and carbon isotopes in the western Eger Rift area (Czech Republic): Relationships with the 2014 seismic activity and indications for recent (2000–2016) magmatic unrest, *Chem. Geol.* **482,** 131–145, doi: 10.1016/j.chemgeo.2018.02.017.

Coutant, O. (1989). Programme de simulation numerique AXITRA, *Rapport L GIT*, Universite Joseph Fourier, Grenoble, France (in French).

Dziewonski, A. M., T. A. Chou, and J. H. Woodhouse (1981). Determination of earthquake source parameters from waveform data for studies of regional and global seismicity, *J. Geophys. Res.* **86,** 2825–2852.

Dziewonski, A. M., G. Ekström, and N. N. Maternovskaya (2001). Centroid moment tensor solutions for July-September 2000, *Phys. Earth Planet. Int.* **124,** 9–23.

Fischer, T., J. Horálek, P. Hrubcová, V. Vavryčuk, K. Bräuer, and H. Kämpf (2014). Intra-continental earthquake swarms in West-Bohemia and Vogtland: A review, *Tectonophysics* **611,** 1–27, doi: 10.1016/j.tecto.2013.11.001.

Fischer, T., J. Horálek, J. Michálek, and A. Boušková (2010). The 2008 West Bohemia earthquake swarm in the light of the WEBNET network, *J. Seismol.* **14,** 665–682.

Ford, S. R., D. S. Dreger, and W. R. Walter (2010). Network sensitivity solutions for regional moment-tensor inversions, *Bull. Seismol. Soc. Am.* **100,** no. 5A, 162–1970.

Hartzell, S. H. (1978). Earthquake aftershocks as Green's functions, *Geophys. Res. Lett.* **5,** 1–4.

Heinicke, J., T. Fischer, R. Gaupp, J. Götze, U. Koch, H. Konietzky, and K.-P. Stanek (2009). Hydrothermal alteration as a trigger mechanism for earthquake swarms: The Vogtland/NW Bohemia region as a case study, *Geophys. J. Int.* **178,** 1–13.

Hrubcová, P., W. H. Geissler, K. Bräuer, V. Vavryčuk, Č. Tomek, and H. Kämpf (2017). Active magmatic underplating in western Eger Rift, Central Europe, *Tectonics* **36,** 2846–2862, doi: 10.1002/2017TC004710.

Ide, S., D. R. Shelly, and G. R. Beroza (2007). Mechanism of deep low frequency earthquakes: Further evidence that deep non-volcanic tremor is generated by shear slip on the plate interface, *Geophys. Res. Lett.* **34,** L03308, doi: 10.1029/2006GL028890.

Irikura, K. (1983). Semi-empirical estimation of strong ground motions during large earthquakes, *Bull. Disaster Prev. Res. Inst., Kyoto Univ.* 33, 63–104.

Jakoubková, H., J. Horálek, and T. Fischer (2018). 2014 mainshock-aftershock activity versus earthquake swarms in West Bohemia, Czech Republic, *Pure Appl. Geophys.* **175,** no. 1, 109–131, doi: 10.1007/s00024-017-1679-7.

Julian, B. R., A. D. Miller, and G. R. Foulger (1998). Non-double-couple earthquakes 1. Theory, *Rev. Geophys.* **36,** 525–549.

Kaempf, H., K. Braeuer, J. Schumann, K. Hahne, and G. Strauch (2013). CO_2 discharge in an active, non-volcanic continental rift area (Czech Republic): Characterisation ($\delta^{13}C$, $^3He/^4He$) and quantification of diffuse and vent CO_2 emissions, *Chem. Geol.* **339,** 71–83, doi: 10.1016/j.chemgeo.2012.08.005.

Kanamori, H. (1979). A semi-empirical approach to prediction of long-period ground motions from great earthquakes, *Bull. Seismol. Soc. Am.* **69,** 1645–1670.

Liao, B.-Y., and H.-C. Huang (2008). Rupture process of the 2002 M_w 7.9 Denali earthquake, Alaska, using a newly devised hybrid blind deconvolution method, *Bull. Seismol. Soc. Am.* **98,** no. 1, 162–179.

Miller, A. D., G. R. Foulger, and B. R. Julian (1998). Non-double-couple earthquakes 2. Observations, *Rev. Geophys.* **36,** 551–568.

Minson, S. E., and D. S. Dreger (2008). Stable inversions for complete moment tensors, *Geophys. J. Int.* **174,** 585–592.

Ohori, M., and Y. Hisada (2011). Comparison of the empirical Green's spatial derivative method and empirical Green's function method, *Bull. Seismol. Soc. Am.* **101,** no. 6, 2872–2886.

Plicka, V., and J. Zahradník (1998). Inverting seismograms of weak events for empirical Green's tensor derivatives, *Geophys. J. Int.* **132,** 471–478.

Plicka, V., and J. Zahradník (2002). The eGf method for dissimilar focal mechanisms: The Athens 1999 earthquake, *Tectonophysics* **359,** 81–95.

Šílený, J. (2009). Resolution of non-double-couple mechanisms: Simulation of hypocenter mislocation and velocity structure mismodeling, *Bull. Seismol. Soc. Am.* **99,** no. 4, 2265–2272.

Šílený, J., and V. Vavryčuk (2002). Can unbiased source be retrieved from anisotropic waveforms by using an isotropic model of the medium? *Tectonophysics* **356,** 125–138, doi: 10.1016/S0040-1951(02)00380-3.

Downloaded from https://pubs.geoscienceworld.org/ssa/srl/article-pdf/91/1/390/4910569/srl-2019154.1.pdf
by Geofyzikalni Ustav Av Cr user

Sokos, E., and J. Zahradník (2008). ISOLA a Fortran code and Matlab GUI to perform multiple point source inversion of seismic data, *Comput. Geosci.* **34,** 967–977.

Stierle, E., M. Bohnhoff, and V. Vavryčuk (2014). Resolution of non-double-couple components in the seismic moment tensor using regional networks: 2. Application to aftershocks of the 1999 M_w 7.4 Izmit earthquake, *Geophys. J. Int.* **196,** no. 3, 1878–1888, doi: 10.1093/gji/ggt503.

Stierle, E., V. Vavryčuk, J. Šílený, and M. Bohnhoff (2014). Resolution of non-double-couple components in the seismic moment tensor using regional networks: 1. A synthetic case study, *Geophys. J. Int.* **196,** 1869–1877, doi: 10.1093/gji/ggt502.

Suzuki, W., and T. Iwata (2009). Broadband seismic wave radiation process of the 2000 western Tottori, Japan, earthquake revealed from wavelet domain inversion, *J. Geophys. Res.* **114,** no. B08302, doi: 10.1029/2008JB006130.

Vavryčuk, V. (2007). Asymptotic Green's function in homogeneous anisotropic viscoelastic media, *Proc. Math. Phys. Sci.* **463,** 2689-2707, doi: 10.1098/rspa.2007.1862.

Vavryčuk, V. (2011a). Principal earthquakes: Theory and observations from the 2008 West Bohemia swarm, *Earth Planet. Sci. Lett.* **305,** 290–296, doi: 10.1016/j.epsl.2011.03.002.

Vavryčuk, V. (2011b). Tensile earthquakes: Theory, modeling, and inversion, *J. Geophys. Res.* **116,** no. B12, doi: 10.1029/2011JB008770.

Vavryčuk, V. (2015). Moment tensor decompositions revisited, *J. Seismol.* **19,** no. 1, 231–252, doi: 10.1007/s10950-014-9463-y.

Vavryčuk, V., and P. Hrubcová (2017). Seismological evidence of fault weakening due to erosion by fluids from observations of intraplate earthquake swarms, *J. Geophys. Res.* **122,** no. 5, 3701–3718, doi: 10.1002/2017JB013958.

Vavryčuk, V., P. Adamová, J. Doubravová, and H. Jakoubková (2017). Moment tensor inversion based on the principal component analysis of waveforms: Method and application to microearthquakes in West Bohemia, Czech Republic, *Seismol. Res. Lett.* **88,** no. 5, 1303–1315, doi: 10.1785/0220170027.

Vavryčuk, V., F. Bouchaala, and T. Fischer (2013). High-resolution fault image from accurate locations and focal mechanisms of the 2008 swarm earthquakes in West Bohemia, Czech Republic, *Tectonophysics* **590,** 189–195, doi: 10.1016/j.tecto.2013.01.025.

Manuscript received 28 June 2019
Published online 13 November 2019

Downloaded from https://pubs.geoscienceworld.org/ssa/srl/article-pdf/91/1/390/4910569/srl-2019154.1.pdf
by Geofyzikalni Ustav Av Cr user